Sulphonamide Chalcones: Conformationally Diverse yet Optically Similar

Jean M. F. Custodio[a]*, Fernando Gotardo[b], Wesley F. Vaz[c], Giulio D. C. D'Oliveira[a], Leandro H. Z. Cocca[b], Ruben D. Fonseca[bd], Caridad Noda Perez[a], Leonardo de Boni[b] and Hamilton B. Napolitano[c]*

[a]Instituto de Química, Universidade Federal de Goias, Goiania, Goias, Brazil

[b]Instituto de Física de São Carlos, Universidade de São Paulo, Sao Paulo, Sao Paulo, Brazil

[c]Ciências Exatas e Tecnológicas, Universidade Estadual de Goiás, Anapolis, Goias, Brazil

[d]Campus Universitario, Universidad Popular del Cesar, Barrio Sabana, Valledupar, Colombia

Correspondence email: jeanmfcustodio@gmail.com; hbnapolitano@gmail.com

Synopsis Three sulphonamide chalcones are characterized. Comparisons between the substitution patterns and optical properties are made.

Abstract

In this paper, we present the synthesis of three chalcone analogues and their spectroscopic, structural and optical characterization. The influence of the different substituents on the crystalline structure and on their optical properties was evaluated. The effects of derivatization on the chalcones, both at the molecular and supramolecular levels, were evaluated. Also, the molar absorptivity, the first hyperpolarizability β and the two-photon absorption cross-section σ_{2PA} were obtained. The extended structures in each compound are stabilized by hydrogen-bonded dimers and by a pseudo-ring formed from an intramolecular H-bond. It was observed that more voluminous substituents, such as chlorine, contribute to the deviation from planarity. Although many effects were observed in molecular structures of these analogues when in solid form, experimental results of linear and nonlinear optical (NLO) properties showed that the optical properties were not as much influenced in solution. In addition, and to support some experimental results, the theoretical first hyperpolarizability was calculated and showed good agreement with experimental results, which are approximately $10 \times 10^{-30}\ cm^5/esu$.

Keywords: crystal structure; sulphonamide chalcones; optics properties

1. Introduction

Chalcones are a class of natural compounds with easy synthesis that have been extensively studied, showing to be promising compounds for diverse applications [1–5]. Optically active materials can be designed and improved from the combination of chalcones with other compounds that also have known application [6–12]. For example, the association of chalcones with coumarins [13,14], imino [15] and indole [16,17] groups have formed new functional hybrid materials. Among them, knowing the molecular structure of sulfonamide chalcones is important when considering their biological applications [18–20]. The crystallographic description of sulfonamide chalcones appears in just a few papers [21–25] and reports of their application as functional materials is also scarce.

There are some examples regarding how structural modifications affect optical properties. Gu and coworkers reported a proportional increase between NLO properties and the electron donor strength [26]. According to da Silva and coworkers, the presence of inter and intramolecular interactions in chalcone co-crystals improves the second harmonic generation efficiency [27]. Also, the relationship between hyperpolarizability values and structural modifications of a chalcone set was studied: the lowest values were found for less conjugated and dimeric systems, while the highest values were found for compounds with strong electron acceptors [28].

In this sense, we sought to determine if there are structural modifications in sulphonamides chalcones that also retain their NLO properties. This paper presents synthesis, crystallographic analysis and optical properties determination of three new hybrid chalcone derivatives consisting of chalcone backbone linked with a sulphonamide group. The three compounds synthesized are: (E)-3-(2-chlorophenyl)-1-(2-(phenylsulfonylamine)phenyl)prop-2-en-1-one (**II**), (E)-3-(2-fluoro-phenyl)-1-(2-(phenylsulfonylamine)phenyl)prop-2-en-1-one (**III**) and (E)-3-(4-fluorophenyl)-1-(2-(phenylsulfonylamine)phenyl)prop-2-en-1-one (**IV**). Considering the different medium of crystal structure determination (solid state) and optical properties (DMSO solution), we also simulated the conformations of **II**, **III** and **IV** in DMSO medium. Finally, the influence of the substitutions was evaluated against on their crystal structures and, in solution, on their optical properties, such as one- and two-photon absorption spectra and molecular second harmonic

generation. Crystallization process of these type of compounds gives the possibility of optical second harmonic generation organic crystals to be employed at the VIS-NIR region, which is the adequate region for optical communications[29–31]

2. Experimental and computational procedures

2.1. Synthesis and Crystallization

2.1.1. General procedures

Compound 2'*N*-phenylsulfonyl acetophenone **I** was synthesized by reaction between benzenesulfonyl chloride and 2-aminoacetophenone in dichloromethane, following literature methods [32]. Three 2-*N*'-sulfonamide chalcones were synthesized (compounds **II** to **IV**) by means of Claisen-Schmidt condensation between the **I** and a substituted benzaldehyde via basic catalysis in ethanolic medium.

2.1.2. Characterization

^{1}H NMR and ^{13}C NMR spectra were recorded by a 400 MHz Bruker Avance III 11.75 T NMR spectrometer. UV-Vis absorption spectra were recorded with a PerkinElmer Frontier Dual Range. FT-IR spectrum was measured in Attenuated Total Reflectance mode in a Spectrum Frontier equipment. Mass spectrometric analyses were performed using a MicrOTOF-Q® III spectrometer equipped with a commercial ESI ion source (Bruker Daltonics, Bremen, Germany). The degree of purity of the compounds was determined from the ^{1}H NMR spectrum, by peak area integration assigned to the structure and the total area of all peaks attributed to the material under analysis. Absorption and fluorescence spectra were measured in the UV-vis-NIR region by using, respectively, a SHIMADSZU UV-1800 and HITACHI F7000 fluorimeter. For both measurements, a 10 mm optical path length fused silica cuvette was filled with sample solution. Chromospheres were dissolved in Dimethyl Sulfoxide (DMSO) in a concentration of about 10^{-5} mol/L.

2.1.3. Synthesis and physicochemical characterization

The synthesis and physicochemical characterization of compound, 1-(2-(phenylsulfonyl-amine)phenyl)ethanone (**I**) and, (*E*)-3-(2-chlorophenyl)-1-(2-(phenylsulfonylamine)phenyl)prop-2-en-1-one (**II**), was reported by Demetrius and coworkers[33]. The synthesis and physicochemical characterization of compounds **III** and **IV** are described below. Claisen-Schmidt condensation reaction between compound I and 2-fluorobenzaldehyde (**III**) and 4-fluorobenzaldehyde (**IV**) was used to synthes compounds **III** and **IV**.

The synthesis of (*E*)-3-(2-fluorophenyl)-1-(2-(phenylsulfonylamine)phenyl)prop-2-en-1-one (**III**) was performed using 20.0 mmol of intermediate **I**, 22.0 mmol of 2-fluorobenzaldehyde and 28.0 mmol of potassium hydroxide as catalyst. The reagents were dissolved in 200 mL of ethanol and stirred at room temperature. After 2.5 h, the reaction was quenched by addition of 37% (w/w) hydrochloric acid in equimolar amounts to potassium hydroxide. The solution was filtered, the precipitate suspended in solution of ethanol and water, and extracted with dichloromethane. The non-aqueous phase was dried with sodium sulfate and allowed to evaporate for crystallization. The crystals were collected and rinsed with ethanol. Yield 54.2 % of a yellow crystalline solid, degree of purity: 97%, mp 136 – 138 ºC. ^{1}H NMR ($CDCl_3$) δ 7.15 (m, 2H); δ 7.21 (t, *J* 7.60 Hz, 1H); δ 7.40 (m, 4H); δ 7.46 (d, *J* 15.85 Hz, 1H); δ 7.50 (t, *J* 7.65 Hz, 1H); δ 7.58 (t, *J* 7.63 Hz, 1H); δ 7.75 (d, *J* 15.80 Hz, 1H); δ 7.76 (d, *J* 8.25 Hz, 1H); δ 7.83 (m, 3H); δ 11.17 (s, 1H) (Fig. S3); ^{13}C NMR ($CDCl_3$) δ 116.41 (d, *J* 21.99 Hz), 120.81, 122.60 (d, *J* 11.31 Hz), 123.24, 124.670 (d, *J* 3.11 Hz), 124.673 (d, *J* 12.70 Hz), 127.24, 129.00, 130.00 (d, *J* 2.58 Hz), 130.73, 132.33 (d, *J* 8.90 Hz), 132.88, 134.48, 138.71, 139.38, 139.94, 161.79 (d, *J* 255.01 Hz) (Fig. S4), 192.86; IR 1645 (m), 1491 (m), 1331 (m), 931 (m), 756 (s); HRMS calculated for $[C_{21}H_{16}FNO_3S+H]^+$ = 382.0913, found 382.0727; $[C_{21}H_{16}FNO_3S+Na]^+$ 404.0733, found 404.0553.

The synthesis of (*E*)-3-(4-fluorophenyl)-1-(2-(phenylsulfonylamine)phenyl)prop-2-en-1-one (**IV**) was performed employing 20.0 mmol of intermediate **I**, 21.7 mmol of 4-fluorobenzaldehyde and 28.0 mmol of potassium hydroxide dissolved in 200 mL of ethanol and stirred at room temperature. After 4.5 h of stirring, the reaction was quenched by addition of 37% (w/w) hydrochloric acid in equimolar amounts to potassium hydroxide. The solution was filtered, the precipitate suspended in solution of ethanol and water, and extracted with dichloromethane. The dichloroethane phase was dried with sodium sulphate and allowed to slowly evaporate for crystallization. The crystals were collected and rinsed with ethanol. Yield, 3.30 g (43.3%) of a yellow crystalline solid, degree of purity of 97%,

mp 136 – 139 ºC. ^{1}H NMR ($CDCl_3$) δ 7.12 (m, ^{3}H); δ 7.28 (d, J 15.55 Hz, ^{1}H); δ 7.39 (m, 2H); δ 7.44 (m, ^{1}H); δ 7.49 (ddd, J 1.46 Hz, 7.26 Hz, 8.46 Hz, ^{1}H); δ 7.60 (m, ^{2}H); δ 7.65 (d, J 15.55 Hz, ^{1}H); δ 7.75 (dd, J 0.67 Hz, 8.38 Hz, ^{1}H); δ 7.83 (m, ^{3}H); δ 11.20 (s, ^{1}H) (Fig. S5); ^{13}C NMR ($CDCl_3$) δ 116.30 (d, J 21.78 Hz), 120.67, 121.75 (d, J 2.25 Hz), 123.16, 124.66, 127.26, 129.00, 130.57 (d, J 8.79 Hz), 130.58, 130.72 (d, J 3.24 Hz), 132.88, 134.42, 139.46, 139.93, 144.68, 164.33 (d, J 252.57 Hz), 192.56 (Fig. S6); IR 1645 (m), 1495 (m), 1332 (m), 930 (m), 744 (m); HRMS calculated for $[C_{21}H_{16}FNO_3S+H]^+$ = 382.0913, found 382.0798; $[C_{21}H_{16}FNO_3S+Na]^+$ 404.0733, found 404.0628.

2.2. Crystallographic characterization

The single crystals selected for crystallographic characterization were obtained by evaporation of dichloromethane in ambient atmosphere for compound **II** and for compounds **III** and **IV** the evaporation of the dichloromethane in an atmosphere rich in ethyl ether was the methodology used to obtain the crystals. The single crystals were mounted in a Bruker APEX II CCD diffractometer with graphite-monochromator MoKα radiation (λ = 0.71073 Å). Data were measured at room temperature. Structure solutions were determined by Direct Methods using SHELXS software [34] and were refined by full-matrix least squares on F^2 using SHELXL2014 software [35]. All hydrogen atoms were placed in calculated positions and refined with fixed individual displacement parameters [U_{iso}(H) = 1.2 or 1.5 U_{eq} (C)] according to the riding model (C–H bond lengths of 0.97 and 0.96 Å for aromatic and methyl groups, respectively). Finally, the chemical parameters were validated by means of Platon [36] and Parst [37] programs throughout the WingX suite [38]. Tables and figures were generated by using Mercury [39] and ORTEP [38] programs. Molecules **II**, **III** and **IV** were deposited in the Cambridge Crystallographic Database Centre (CCDC) under codes 1868826, 1868827 and 1868828, respectively. Using the software Gaussian, the conformations of II, III and IV were simulated for DMSO medium and they were found to be similar, so that the crystal structural properties can be extended to the aqueous medium.

2.3. Nonlinear optical measurements

2.3.1. Two-Photon Absorption

Two-photon absorption (2PA) cross section spectra were determined by employing tunable femtosecond Z-Scan technique [40]. This technique allows the quantification of the 2PA cross section by monitoring the sample transmittance. The sample is translated along (z-direction) a focused intense laser beam. Changes in the optical transmittance are acquired as a function of the sample position (Z). Consequently, around the focus, the transmittance of the laser by the sample decreases proportionally to the induced 2PA. Further from the focal region, the laser intensity diminishes and the nonlinear optical effects (2PA) are not induced, resulting in only linear optical transmittance. The ratio between the transmittance for each Z-position to the transmittance away from the focus is defined as the normalized transmittance (T(z)), from which the 2PA cross section can be evaluated by employing Eq. (1). Further details see: [40].

In our experimental setup, a tunable optical parametric amplifier (TOPAS), pumped by a Ti:Sapphire (CPA-2001 system from Clark-MXR Inc.) laser with 150 fs pulse width at 775 nm, operating at 1 kHz repetition rate is used. This device delivers tunable wavelengths from 470 nm up to 2000 nm with 120 fs pulse width, operating at a 1 kHz repetition rate. The laser beam is focused by a 15 cm convergent lens at the Z-Scan experimental setup. The sample is positioned and translated with respect to the focused beam, and the transmitted light is registered by a Silicon photodetector for each Z-position of the sample. The signal is amplified and averaged by a commercial locking amplifier in order to increase the signal/noise ratio. Once the normalized transmittance Z-Scan signature is obtained, the 2PA cross section is determined by fitting T(Z) to Eq. 1 [40]:

$$T(Z) = \frac{1}{\sqrt{\pi} q_0(Z,0)} \int_{-\infty}^{\infty} \ln[1 + q_0(Z,0) e^{-t^2}] dt \quad (1).$$

The sample position is defined by Z, q_0 is given by $q_0 = \alpha_{2PA} I_0 L \, (1 + Z^2/Z_0^2)^{-1}$. I_0 is the pulse intensity, Z_0 is the Rayleigh length and, finally, L is the sample optical path. 2PA cross section is defined by $\sigma_{2PA} = (\hbar\omega/N)\alpha_{2PA}$, in which α_{2PA} is the nonlinear absorption coefficient, $\hbar$ is the Planck constant, ω is the light frequency, and N is the number of molecule per cm^3. To quantify the σ^{TPA}, we usually use $1\ GM = 1 \times 10^{-50}\ cm^4\ s\ photon^{-1}$ (Göppert-Mayer

unit (GM); [41]. This procedure was performed at different wavelengths in order to obtain the 2PA spectrum of each sample.

2.3.2. First order hyperpolarizability

To determine the first hyperpolarizability (β) of each chalcone [42], we employed the Hyper Rayleigh scattering (HRS) technique [42,43]. For this, we use a Nd:YAG Q-Switched mode-locked laser with pulses at 1064 nm (ω). This configuration delivers an envelope about 300 ns which contains of about 30 pulses of 100 ps, these pulses in the envelope are separated by 13.2 ns from each one [43]. Laser was set to operate at 100 Hz of repetition rate. Pulses are focalized at the samples and the scattered optical second harmonic at 532 nm (2ω) was collected by a photomultiplier tube positioned perpendicular to the incident beam (1064 nm). It is important to highlight that we used an optical filter centered at 532nm with 10 nm of bandwidth at the photomultiplier window to ensure that only the nonlinear scattered signal is detected by the photomultiplier. The second harmonic scattered signal I(2ω) is related to the laser intensity I(ω) by the following expression:

$$I(2\omega) = G \sum_{i=1}^{M} N_i \beta_i^2 I^2(\omega) \qquad (2).$$

In this equation, N_i is the molecular concentration, G is a constant instrumental factor. G depends on the laser beam and experimental setup and can be determined using a sample with a known β value; in this case, we use *para*-nitroaniline (pNA) dissolved in DMSO, $\beta(1064\ \text{nm}) = 25.3 \times 10^{-30} \text{cm}^5/\text{esu}$ [43]. It is important to emphasize here that chalcones and pNA were dissolved in high concentration in DMSO solvent. Thus, it was possible to determine β of the three chalcone derivatives measuring I(2ω) for several N_i. A linear relation between I(2ω) and N_i is obtained, and the angular coefficient of it, α_{chalcone}, is related to β_{chalcone} by E.q 3

$$\beta_{\text{chalcone}} = \sqrt{\beta_{\text{pNA}}^2 \frac{\alpha_{\text{chalcone}}}{\alpha_{\text{pNA}}}} \qquad (3)$$

in which, $\alpha_{chalcone} = G\beta^2_{chalcone}$ and $\alpha_{pNA} = G\beta^2_{pNA}$.

3. Results and discussion

3.1. Molecular Structure of Compound II

The compound **II** is a chalcone with a chlorine atom and phenyl-sulfonamide group *ortho*-bonded to aromatic rings A and B, respectively (Fig. 1a). It crystallizes in the monoclinic centrosymmetric space group $P2_1/c$ (Table 1). The angle formed by the mean plane of the chalcone rings A and B is 42.59(5)°, demonstrating a significant deviation from co-planarity. This is supported by the Cl1–C1–C9–O1 dihedral angle ω1 = 31.07(13)°, which shows a synclinal conformation of the chlorine group with respect to carbonyl group.

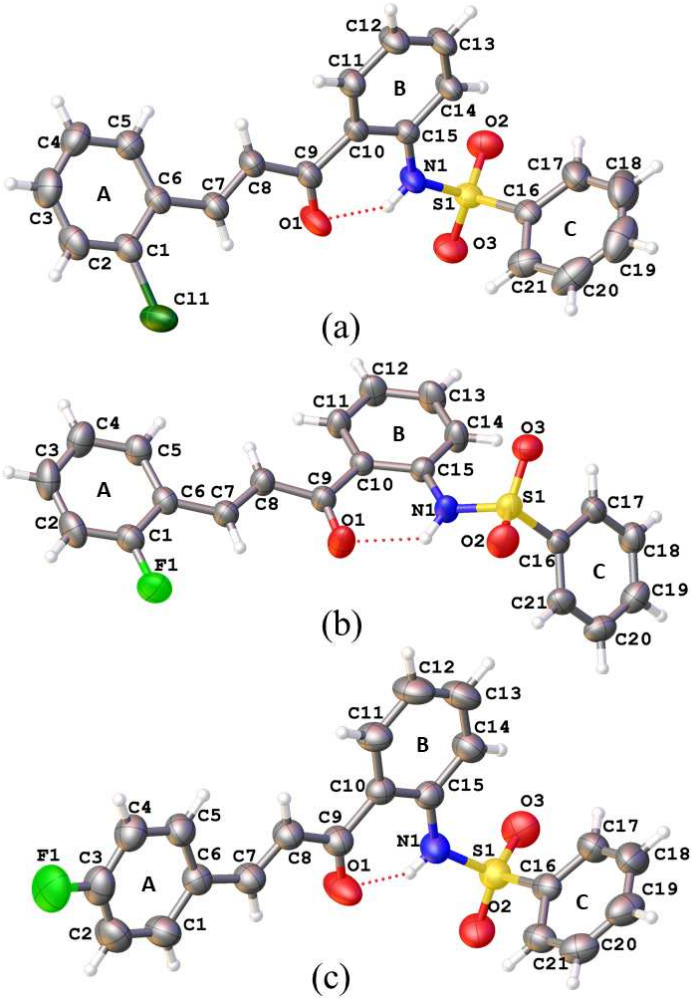

Figure 1 50% probability ellipsoid plot of **II** (a), **III** (b) and **IV** (c). Non-hydrogen atoms are arbitrarily labelled, and hydrogen atoms are shown as spheres of arbitrary radii.

Table 1 Experimental details

	(**II**)	(**III**)	(**IV**)
Crystal data			
Chemical formula	$C_{21}H_{16}ClNO_3S$	$C_{21}H_{16}FNO_3S$	$C_{21}H_{16}FNO_3S$
M_r	397.86	381.41	381.41
Crystal system, space group	Monoclinic, $P2_1/c$	Monoclinic, $C2/c$	Monoclinic, $P2_1/c$
Temperature (K)	296	296	296
a, b, c (Å)	13.7952 (7), 7.5840 (4), 20.2728 (9)	26.984 (3), 7.6486 (8), 18.354 (2)	13.1059 (5), 17.5044 (8), 8.1948 (4)
β (°)	62.896 (3)	107.479 (3)	102.278 (2)
V (Å^3)	1888.07 (17)	3613.2 (7)	1836.98 (14)
Z	4	8	4
Radiation type	Mo $K\alpha$	Mo $K\alpha$	Mo $K\alpha$
μ (mm^{-1})	0.33	0.21	0.21
Crystal size (mm)	0.74 × 0.46 × 0.34	0.10 × 0.10 × 0.08	0.65 × 0.22 × 0.21
Data collection			
Diffractometer	Bruker *APEX*-II CCD	Bruker *APEX*-II CCD	Bruker *APEX*-II CCD
Absorption correction	–	–	–
No. of measured, independent and observed [$I > 2\sigma(I)$] reflections	27435, 3880, 3394	24691, 3749, 2712	23587, 3762, 2982
R_{int}	0.035	0.054	0.033
$(\sin\theta/\lambda)_{max}$ (Å^{-1})	0.626	0.630	0.626
Refinement			
$R[F^2 > 2\sigma(F^2)]$, $wR(F^2)$, S	0.038, 0.106, 1.04	0.045, 0.132, 1.06	0.040, 0.110, 1.04
No. of reflections	3880	3749	3762
No. of parameters	259	256	263
H-atom treatment	H atoms treated by a mixture of independent and constrained refinement	H atoms treated by a mixture of independent and constrained refinement	H atoms treated by a mixture of independent and constrained refinement
$\Delta\rho_{max}$, $\Delta\rho_{min}$ (e Å^{-3})	0.27, –0.33	0.30, –0.31	0.32, –0.28

Computer programs: *SHELXL2016*/6 (Sheldrick, 2016).

Only C–H···O intermolecular interactions are observed stabilizing the crystal packing of **II**. Two molecules are assembled in a dimeric arrangement by a $R_2^2(18)$ motif involving carbonyl group and aromatic ring C (Fig. 2a). These dimers are joined together by means of a bifurcated interaction which an $O_{sulfonyl}$ atom serves as an acceptor from two carbon atoms in a $C_2^1(8)[R_2^1(6)]$ motif (Fig. 2b). Finally, the supramolecular arrangement of **II** is stabilized by one more C–H···O interaction involving the sulfonyl group and the aromatic ring A in a $C(11)$ motif giving rise to a 1D chain running parallel to [001] (Table 2).

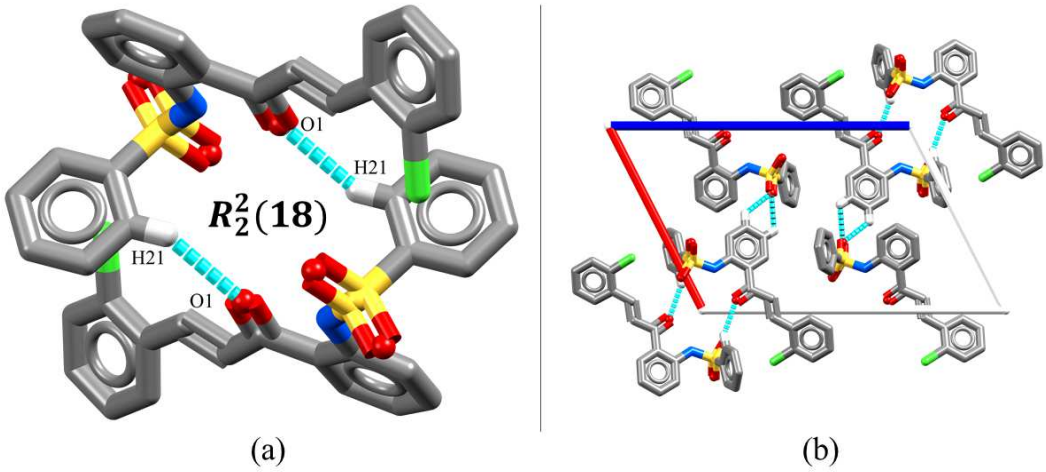

Figure 2 Dimer formed by two molecules **II** (a) and its crystal packing (b)

Table 2 Hydrogen-bond geometry (Å, º) for (II)

D—H···*A*	*D*—H	H···*A*	*D*···*A*	*D*—H···*A*
C5—H5···O3^{i}	0.95 (2)	2.58 (2)	3.342 (2)	137.1 (16)
C21—H21···O1^{ii}	0.92 (2)	2.53 (2)	3.320 (2)	144.1 (17)
C12—H12···O2^{iii}	0.98 (2)	2.70 (2)	3.274 (2)	118.1 (15)
C13—H13···O2^{iii}	0.94 (2)	2.59 (2)	3.255 (2)	128.5 (16)

Symmetry codes: (i) *x*, −*y*+1/2, *z*−1/2; (ii) −*x*, −*y*+1, −*z*+1; (iii) −*x*+1, *y*+1/2, −*z*+1/2.

3.2. Substituent effect on the crystal structure

We evaluated substitution effects by comparing the crystal structures of **II** and **III**, which differs only by the atom bonded to the ring A. Compound **III** substitutes fluorine for the chlorine

atom in **II** (Fig. 1b). **III** crystallizes in the C-centered monoclinic space group C_2/c (Table 1). Figure 3 shows a molecular overlay obtained by mapping the aromatic ring B from molecules **II** and **III**. The main structural difference is the planarity of the chalcone moiety. For **III**, the angle formed between aromatic rings A and B is smaller than **II** ($\measuredangle$ = 20.37(10)°), as result of reduction of steric repulsion between the fluorine and carbonyl group and n···π donation differences of fluorine and chlorine atoms. Since chlorine atom has a greater atomic radius, this repulsion is greater in **II** [44].

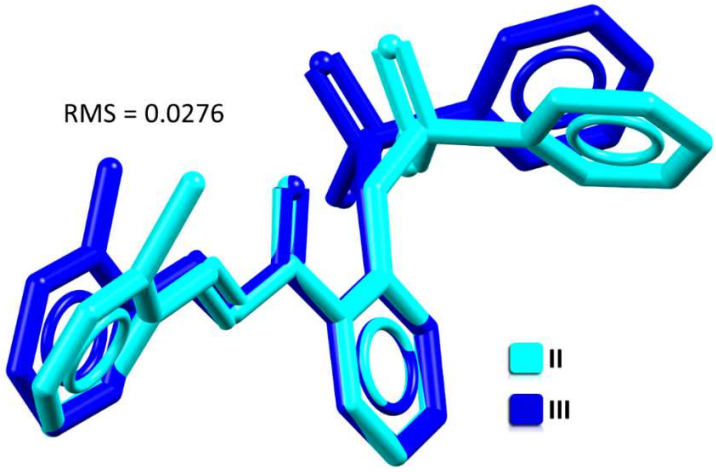

Figure 3 Overlapping obtained by fixing the aromatic ring B from molecules **II** (cyan color) and **III** (blue color).

Similar to **II**, the crystal packing of **III** is also composed by dimers (Fig. 4). There is a dimer with $R_2^2(16)$ motif (blue color, in Fig. 4) involving sulfonyl group and olefinic hydrogen. A 1D chain is formed by assembling these dimers in a second order $R_4^4(16)$ ring motif (pink color, in Fig. 4) parallel to [101]. The last C–H···O interaction observed in the crystal packing of **III** involves the carbonyl group and the aromatic ring C and contributes to 3D arrangement of **III** (Table 3).

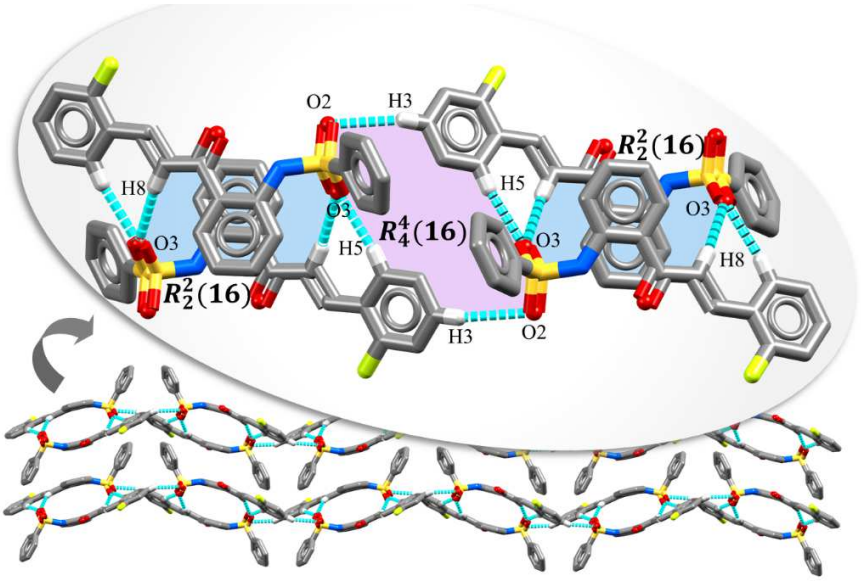

Figure 4 Crystal packing of **III**, evidencing the supramolecular arrangement composed by two dimers with $R_2^2(16)$ ring motif (blue) joined by a $R_2^2(16)$motif (pink)

Table 3 Hydrogen-bond geometry (Å, º) for (**III**)

D—H···*A*	*D*—H	H···*A*	*D*···*A*	*D*—H···*A*
C3—H3···O2^{i}	0.95 (3)	2.69 (3)	3.577 (3)	156 (3)
C5—H5···O3^{ii}	0.97 (3)	2.51 (3)	3.466 (3)	169 (2)
C8—H8···O3^{ii}	0.96 (3)	2.55 (3)	3.475 (3)	163 (2)
C20—H20···O1^{iii}	0.88 (3)	2.73 (3)	3.273 (3)	121 (2)

Symmetry codes: (i) *x*−1/2, −*y*+3/2, *z*−1/2; (ii) −*x*+1/2, −*y*+3/2, −*z*; (iii) −*x*+1/2, *y*−1/2, −*z*+1/2.

3.3. Positional effect on the crystal structure

The positional effect is evaluated by comparing the crystal structures of **III** and **IV**, which differs only by the position of the atom bonded to aromatic ring A. Similarly to **III**, the structural isomer **IV** also has a fluorine atom bonded to the aromatic A, but in the *para* position (Fig. 1c). It crystallizes in the primitive monoclinic space group $P2_1/c$ (Table 1).

Structural differences between **III** and **IV** are demonstrated in Figure 5. Compound **IV** has a more planar chalcone moiety than compound **III**, as confirmed from the angle formed by its aromatic rings A and B ($\measuredangle$ = 3.32°). This difference is again from a reduction of the electron-electron repulsion of fluorine atom and carbonyl group. Since **III** has an *ortho*-bonded fluorine atom, this repulsion is stronger than in **IV**, causing the deviation from planarity [44].

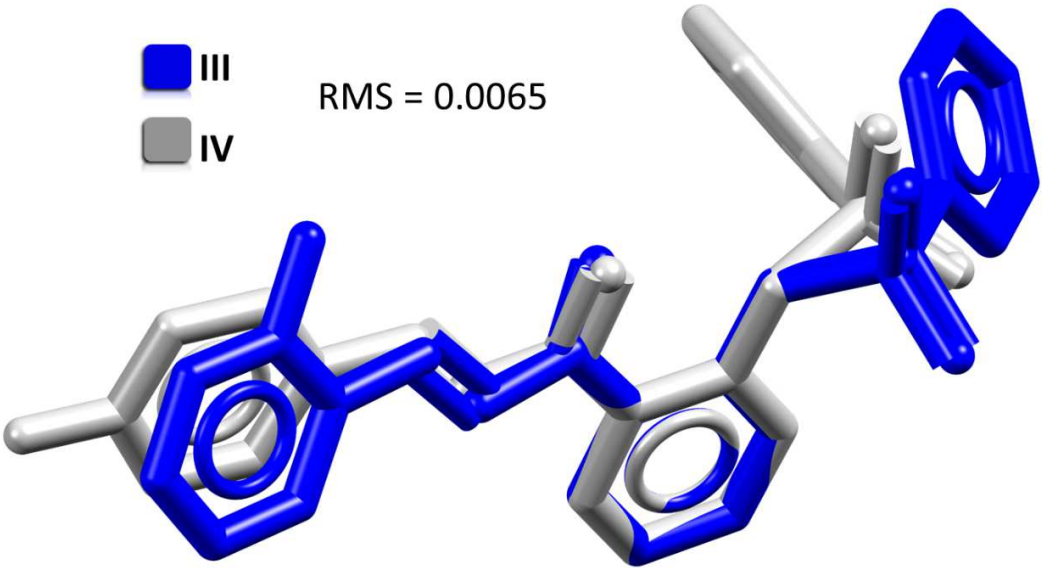

Figure 5 Overlapping obtained by fixing the aromatic ring B from molecules **III** (blue color) and **IV** (gray color).

Carbonyl group and aromatic ring C are assembled into centrosymmetric dimers with $R_2^2(20)$ motif (Fig. 6a). Also observed is a 1D chain formation involving the aromatic ring B and the sulfonyl group in a $C(11)$ motif running along [010]. These chains are assembled in a 3D arrangement by means of $C_{aromatic}$–H···$O_{sulfonyl}$ and $C_{aromatic}$–H···$O_{sulfonyl}$ interactions (Fig. 6b); (Table 4).

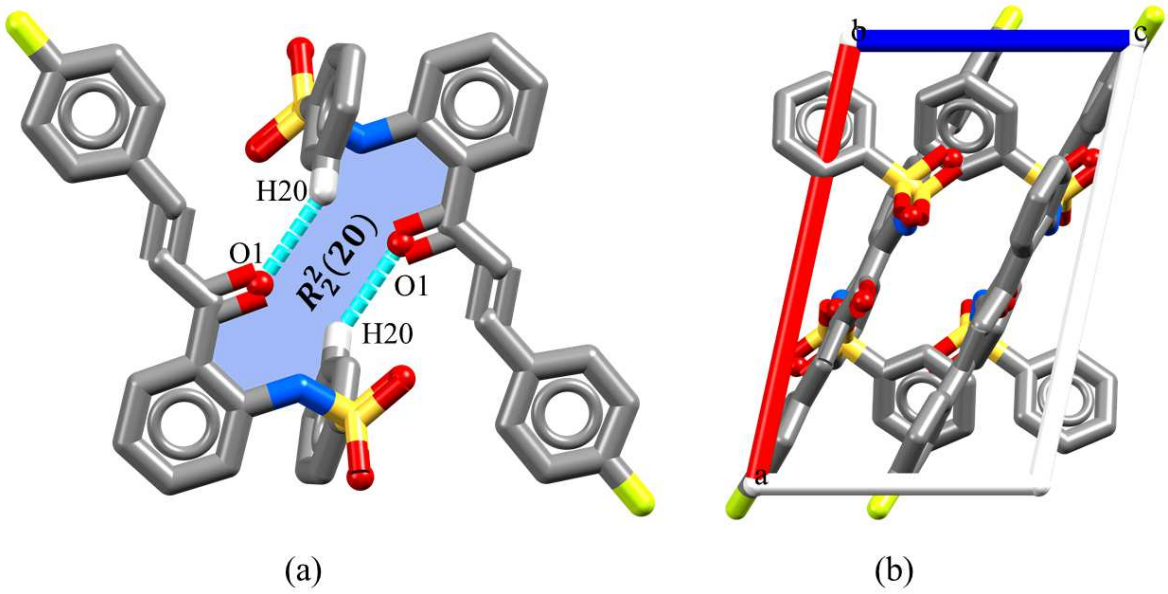

Figure 6 Dimer formed by two molecules **IV** (a) and its crystal packing (b)

Table 4 Hydrogen-bond geometry (Å, º) for (**IV**)

D—H···*A*	*D*—H	H···*A*	*D*···*A*	*D*—H···*A*
C20—H20···O1^{i}	0.94 (3)	2.64 (3)	3.317 (3)	129.2 (19)
C5—H5···O2^{ii}	0.92 (3)	2.67 (3)	3.590 (2)	174 (2)
C20—H20···O3^{iii}	0.94 (3)	2.71 (3)	3.416 (2)	132.3 (19)
C19—H19···F1^{iv}	0.93 (3)	2.64 (3)	3.375 (3)	136.0 (19)

Symmetry codes: (i) −*x*+1, −*y*, −*z*; (ii) −*x*+1, *y*+1/2, −*z*+1/2; (iii) *x*, *y*, *z*−1; (iv) *x*−1, −*y*+1/2, *z*−1/2.

3.4. One-, two-photon absorption spectra and first order hyperpolarizabilities

Figure 7 shows molar absorptivity (dashed blue lines) of the three chalcone derivatives dissolved in DMSO solvent at room temperature. One can see that the lower transition band is located at approximately 318 nm with a molar absorptivity of about 16500 L mol^{-1} cm^{-1} to the derivatives shown in (a) and (c) and about 19500 L mol^{-1} cm^{-1} for (b). Changes in the atoms, from chlorine to fluorine and from *ortho* to *para* position, did not significantly change the energy of the lowest energetic band and the molar absorptivity magnitude, when comparing the compounds. All three compounds dissolved in DMSO are transparent at wavelengths longer than 400 nm. Fluorescence emission was not evidenced for these samples, which indicates a nonradiative relaxation process from first singlet excited state to the ground state[45].

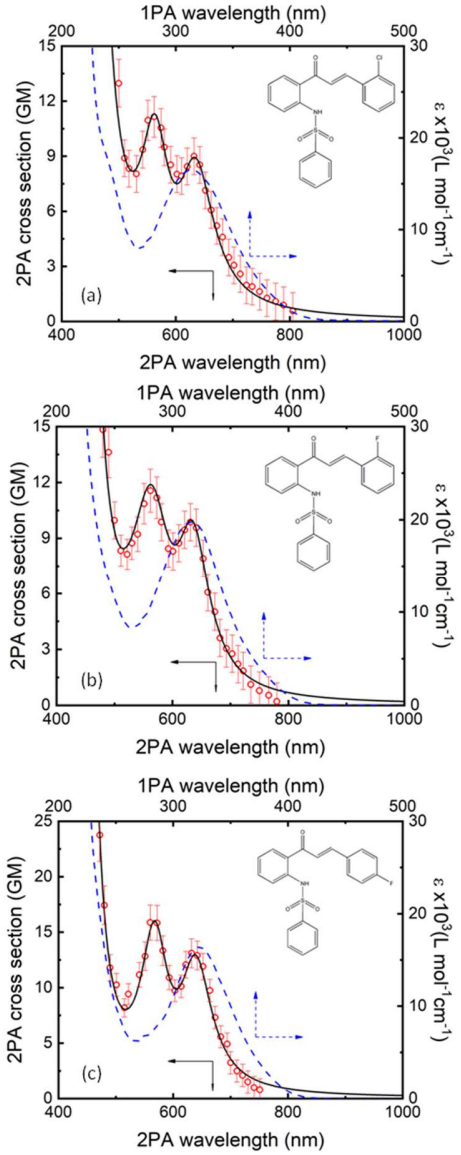

Figure 7 Linear absorption (ε) (dashed blue lines) and two-photon absorption (open red circles) spectra of all three chalcone derivatives dissolved in DMSO solvent. The black line is the adjustments obtained with Sum-Over-States model. The inset shows the molecular structure of the derivatives.

Figure 7 also depicts 2PA spectra (open red circles) of all three chalcones obtained with fs-tunable Z-Scan technique. Each point of the spectrum represents the two-photon absorption cross section calculated from Eq. (1). Similar to the 1PA spectrum, 2PA spectra are not significantly different across the compounds. The maximum 2PA cross sections are of the same order of magnitude. For all compounds, two 2PA bands appear located at

approximately 565 nm and 635 nm. The latter corresponds to the same transition allowed by 1PA (~ 318 nm). The other, located at 565 nm, represents a state located at approximately 255 nm, which has no similar 1PA. For wavelengths shorter than 500 nm, the 2PA cross sections increase due to the one-photon resonance enhancement. Similarities in the 1PA and 2PA between the compounds could be understood by the molecular structures. The chalcone moiety, which has the same π-conjugated characteristics, is responsible for the one- and two-photon absorption bands centered at approximately 318 nm (636 nm) in all compounds. The replacement of the chlorine atom to the fluorine, which has the higher electronegativity, do not affect considerable the 1PA and 2PA spectra between the molecules.

It is important to mention here than by using both 1PA and 2PA spectra combined, we could estimate information about the magnitude of some electronic properties, such as the transition dipole moments and permanent dipole moment difference between the ground and first excited states ($\Delta\vec{\mu}_{01} = \vec{\mu}_{11} - \vec{\mu}_{00}$). For example, the transitions dipole moment from the ground to the first excited state (μ_{01}) is determined by [46]:

$$\mu_{01}{}^2 = \frac{3\cdot 10^3 \ln(10)\hbar c}{(2\pi)^3 N_A \omega_{01}} \frac{n}{L^2} \int \varepsilon(\omega) d\omega \qquad (4),$$

in which, N_A is Avogadro's number, $\hbar$ is Planck's constant, c is the speed of light, and ω_{01} represents the transition frequency of the first excited state. $L = 3n^2/(2n^2 + 1)$ describes the Onsager local field factor, which represents the surround medium effect of the solvent to the solute[47], that in the present work is DMSO solvent, with a refractive index (n) equal to 1.42. In Equation (4), $\varepsilon(\omega)$ is the molar absorptivity, obtained from the linear absorption measurements.

Combining μ_{01}, determined directly from the linear absorption spectrum, with some other spectroscopic parameters, the experimental 2PA spectrum can be modeled with Sum-Over-States (SOS) approach. In Figure 7, the solid black lines represent a construction of the experimental 2PA (open circles) with SOS model, which is given by the following expression [48,49]:

$$\sigma_{2PA}^{SOS}(\omega) = \frac{128}{5}\frac{\pi^5}{(chn)^2}L^4\frac{\omega^2}{(\omega_{01}-\omega)^2+\Gamma_{01}^2}\left[\frac{|\mu_{01}|^2\Delta\mu_{01}^2\Gamma_{01}}{(\omega_{01}-2\omega)^2+\Gamma_{01}^2}+\frac{|\mu_{12}|^2|\mu_{01}|^2\Gamma_{02}}{(\omega_{02}-2\omega)^2+\Gamma_{02}^2}+\frac{|\mu_{13}|^2|\mu_{01}|^2\Gamma_{03}}{(\omega_{03}-2\omega)^2+\Gamma_{03}^2}\right] \quad (5)$$

in which, ω is the frequency of the laser. ω_{0n} and Γ_{0n} are, respectively, the transition frequency and damping constant of the $0 \rightarrow n$ transition (n=1,2,3). It is important to mention here that the three terms, inside of the brackets, describe the electronic transitions observed in the 2PA experimental spectrum. In all terms, one can notice the product between the dipole moments in the numerator, in which all have μ_{01} in common, an input parameter obtained from the linear absorption spectra. It ensures that each term in the brackets is independent and only one dipole parameter is adjusted per term. In summary, Table 5 presents the parameters obtained with both 1PA and 2PA spectra combined with Eq. 4 and Eq. 5. The damping constants were used to be Γ_{0n} = 0.3 eV, which is common, in most cases, to describe electronic transitions for organic molecules at the UV-VIS region. These parameters are close in magnitude, which indicates that the charge distribution at the ground and excited state are similar between the molecules.

Values in Table 5 and the magnitude of the 2PA cross section shown in Figure 7, taking in consideration the experimental error, are close to those reported in the literature for chalcone-based compounds, which were obtained by using similar methodology of measurements[45,50–53]. Values in Table 5 and the magnitude of the 2PA cross section shown in Figure 7, taking in consideration the experimental error, are close to those reported in the literature for chalcone-based compounds, which were obtained by using similar methodology of measurements [45,50–53], as the ones employed in the present work. For example, ref. 48 presents a similar study in two substituted chalcones employing similar fs Z-Scan experiment to determine the 2PA cross-sections. Results have shown similar 2PA cross-sections between the chalcone molecules. The magnitudes observed for the 2PA cross-section in the lower energetic band are close (~ 15 GM) to the ones showed here. It is interesting to point out that the 2PA band located at 565 nm for molecules **II**, **III** and **IV**, have no similar band in the case of Ref. 48. One explanation for it is the presence of the phenylsulfonylamine group attached to the main chalcone moiety in our molecules. Santos at al.[X] studied two-photon absorption spectrum in bromo- and chloro-derivatives of

dibenzylideneacetone and obtained a maximum value of about 25 GM for the molecule containing bromine and 17 GM for the one with chlorine atom. Lemes et al.[51] presented a similar study in a chalcone derivative with a chlorine atom in the *para* position and also with twice the conjugation length when compared to our molecules. In that work, a maximum 2PA cross-section of about 30 GM was observed. The increase in the 2PA magnitude comparing to the present molecules is explained by the conjugation length be greater. Custodio et al studied two-photon absorption spectrum of a bromine sulfonamide chalcone[52], with a similar molecular structure to the ones presented here. 2PA maximum cross-section value of 10 GM was obtained for the lower energetic band. A blue shifted in the one- and two-photon absorption spectrum is observed when compared to the sulphonamide chalcone presented here. It can be understood by the presence of bromine atom, which is less electronegative than chlorine and fluorine atoms. Moreover, it is important to describe that for bromine sulfonamide chalcone, the overlap between the two 2PA bands have increased. It indicates that charge distribution in the phenylsulfonylamine group attached to the main chalcone moiety may not suffer influence replacing bromine by chlorine or fluorine atoms.

Table 5 Transitions dipole moments and permanent dipole moment difference for the three compounds studied in this work, in Debyes unit.

Chalcone derivatives	μ_{01}	$\Delta\mu_{01}$	μ_{12}	μ_{13}
II	6.4	4.6	4.0	4.0
III	7.2	3.8	4.1	4.5
IV	6.5	5.2	4.4	4.5

Concerning to the molecular second harmonic generation measurements, which are related to the first order hyperpolarizability (β) of the molecule, the values of chalcone derivatives were determined after the experimental setup was calibrated with pNA (standard compound) dissolved in the same solvent. As it was shown in the molecular structure, one can see that all three chalcones derivatives are noncentrosymmetrical molecules in terms of charge distribution. It because of the different donor-acceptor groups attached to the main chalcone moiety. Consequently, when the molecules are in solution and not crystallized, it is expected to observe a very low incoherent second-order signal

from each individual molecule that can be measured by using HRS technique. The measured scattered nonlinear signal (532 nm) shows a quadratic dependence with the pump intensity (1064 nm), indicating that two photons of 1064 nm are annihilated in order to generate one of 532 nm. It can be visualized at the left hand inset in Fig. 8, as example, for compound **III**. The solid line, for each curve, represents the best second order polynomial fit. Also, in Fig. 8, it is presented the linear dependence of $I(2\omega)/I^2(\omega)$ (open symbols) as a function of five molecular concentrations for **II**, **III**, **IV** derivatives, as well as pNA molecule. Lines in these graphs represent the best linear fits, in which the angular coefficients, when compared with the pNA, provide β values for the studied samples, all calculated from Eq. (3).

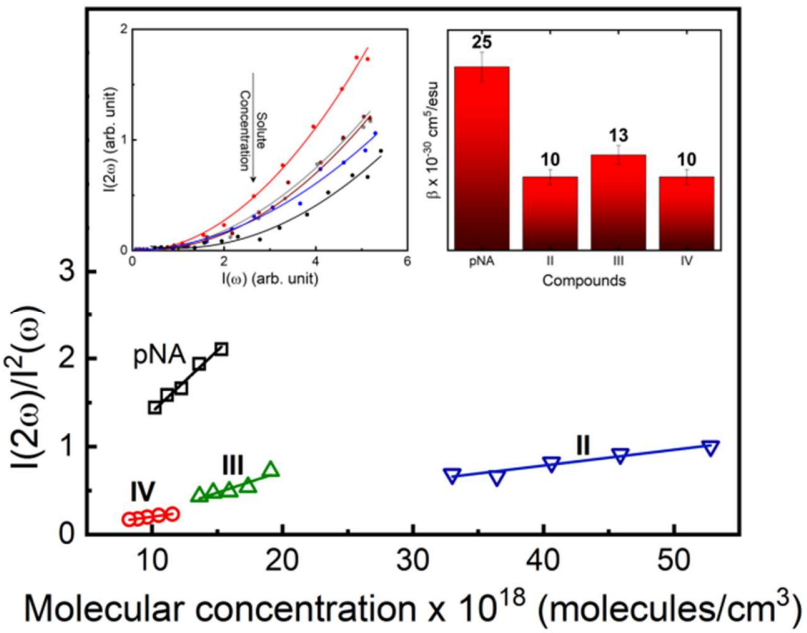

Figure 8 Linear dependence of $I(2\omega)/I^2(\omega)$ as function of the molecular concentrations for pNA (squares) and chalcone derivatives: **II** (blue triangle), **III** (green triangle and **IV** (circles). Lines represent the linear fits. The inset, at left side, represents the first hyperpolarizability scattering signals as a function of the pump intensity for five distinct molar concentrations of sample **III**. Lines are the best second order polynomial fits. Similar curves were obtained for the other compounds. The inset, at right side, depicted the β values for all compounds and pNA.

The results obtained for all three compounds showed that values of β are similar to each other of approximately 1x10^{-29} cm^5/esu. This nonlinear optical effect agrees with the other optical characteristics, such as linear absorption and 2PA spectra. In other words, as can be seen, linear and 2PA spectra are all similar across all three chalcones analysed. Consequently, it is expected that β´s are similar when comparing the three compounds studied here. β values at 1064 nm for **II**, **III** and **IV** can be indirectly estimated by employing a simplified two-level model [54], taking in consideration properties obtained from the one- and two-photon absorptions. In this model, $\Delta\mu_{01}$ and μ_{01} (presented at Table 5), were used in this approach to first determine the static first-order hyperpolarizability (β_0) by employing the following expression:

$$\beta_0(0;0,0) = \frac{3}{2}\frac{|\mu_{01}|^2|\Delta\mu_{01}|}{(\hbar\omega_{01})^2} \qquad (6),$$

in which, $\hbar\omega_{01}$ is the energy of the first electronic transition, in the present case to be approximately 3.88 eV for all three compounds, because the lower electronic transition is at the approximately same wavelength. The estimated static first-order hyperpolarizabilities are 7.3, 7.7 and 8.5 x10^{-30} cm^5/esu, respectively, for compounds **II**, **III** and **IV**.

To calculate the dynamical β and thus compare to the experimental ones, one can take into account the resonance enhancement effect due to the optical frequency dispersion, it can be evaluated by using the undamped two-level model [54–56]. With this simplified model, the dynamic hyperpolarizabilities of the compounds were extrapolated at the incident laser frequency (ω), which is far from the first excited state ($\hbar\omega_{01}$), by using [54]:

$$\beta(-2\omega;\omega,\omega) = \frac{\omega_{01}^4}{(\omega_{01}^2-4\omega^2)(\omega_{01}^2-\omega v^2)}\beta_0 \qquad (7).$$

In Figure 9, the experimental values obtained with the HRS technique (symbols) are compared to the ones obtained with the undamped two-level model (solid lines), the latter calculated by using 1PA and 2PA experiments. One can see a good agreement between both results at approximately 1.16 eV (~ 1064 nm). At 1.16 eV, the values obtained with Eq. 7 are 12.6 (1.26 times higher), 13.3 (1.02 times higher) and 14.7 x10^{-30} cm^5/esu (1.47 times higher), respectively, for compounds **II**, **III** and **IV**.

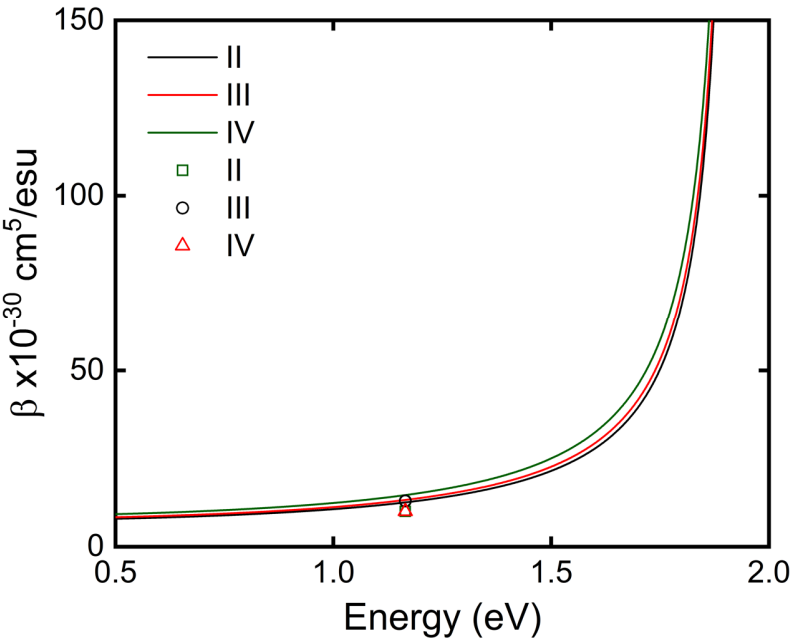

Figure 9 Experimental HRS signal measured at 1064 nm (~ 1.16eV) (symbols) and simplified two-level dispersion model (lines) for **II**, **III** and **IV**.

Values of the molecular optical second harmonic are in the same order of magnitude to the ones found in the literature for chalcone-based compounds [45,50–53]. In that works, a similar HRS experimental methodology was employed. For example, Abegão et al[48] determined values of the molecular second order nonlinear response of about two times higher than the ones reported here, for two substituted chalcones dissolved in methanol. Also, a chalcone derivative with a chlorine atom in the *para* position and with twice the conjugation length showed a value of about 22 $\times 10^{-30}$ cm^5/esu, obtained also at 1064 nm[51]. Custodio et al[52] determined for a bromine sulfonamide chalcone a value similar to the ones presented here. Santos et al[53] studied bromo- and chloro-derivatives of dibenzylideneacetone, in which the molecules presented a conjugation length longer than ours chalcones. The results obtained for the molecular second-order nonlinear response were 25 and 27 $\times 10^{-30}$ cm^5/esu respectively for bromine and chlorine dibenzylideneacetone. The results reported in the literature, by using similar methodology, have shown that chalcones molecules present similar values of first order hyperpolarizability. An augment of β magnitude can be understood by an increase in the conjugation length of the molecule associated to the presence of donor-acceptor groups, which defined a noncentrosymmetric charge distribution.

4. Conclusions

The substituent effect on crystal structures was measured by comparison of molecules **II** and **III**, which differ only by the atom bonded to the ring A. For **III**, the angle formed by aromatic rings A and B was found to be smaller than **II**, evidencing the planarity deviation observed due to the greater atomic radius of chlorine. In addition, the positional effect on the crystal structure was evaluated after comparing the isomers **III** and **IV**. The *para* substitution observed in **IV** contributed to the planarity of its chalcone backbone, due to its lower steric repulsion when compared to **III**, a *ortho*-substituted chalcone. Finally, crystal packing of the molecules was found to be stabilized by dimers and by a pseudo-ring formed from an intramolecular H-bond. Although slightly different structural conformations were observed for the molecules **II**, **III** and **IV** at solid state, experimental results from linear and nonlinear optical measurements in solution showed that the values of optical effects are not significantly influenced by these structural modifications. Considering the nonlinear optical properties, estimated first hyperpolarizabilities (β´s), by employing parameters obtained from distinct spectroscopic techniques, are in good agreement with the ones experimentally obtained with Hyper Rayleigh scattering technique, which are approximately $10 \times 10^{-30}\ cm^5/esu$.

5. Supporting Information

^{1}H and $^{13}C\{^{1}H\}$ NMR spectrum (500 MHz, $CDCl_3$), of compounds **II**, **III** and **IV**.

Acknowledgements

The authors are grateful to Professor Allen Oliver for his collaboration in reading this manuscript. The authors also acknowledge the financial support of the Conselho Nacional de Desenvolvimento Científico e Tecnológico (CNPq), Fundação de Amparo à Pesquisa do Estado de Goiás (FAPEG), INCT-FOTÔNICA, FAPESP 2016/20886-1 and 2018/11283-7, Army Research Laboratory W911NF-17-1-0123 and Air Force Office of Scientific Research (FA9550-12-1-0028). This study was financed in part by the Coordenação de Aperfeiçoamento de Pessoal de Nível Superior - Brasil (CAPES) - Finance Code 001..

References

(1) Zhu, X.; Yin, F.; Zhao, H.; Chen, S.; Bian, Z. Some New Azobenzene Liquid Crystals Involving Chalcone and Ester Linkages. *RSC Adv.* **2017**, *7* (73), 46344–46353. https://doi.org/10.1039/C7RA06958H.

(2) Tan, J.; Zhang, Y.; Zhang, M.; Tian, X.; Wang, Y.; Li, S.; Wang, C.; Zhou, H.; Yang, J.; Tian, Y.; et al. Small Molecules of Chalcone Derivatives with High Two-Photon Absorption Activities in the near-IR Region. *J. Mater. Chem. C* **2016**, *4* (15), 3256–3267. https://doi.org/10.1039/C6TC00382F.

(3) Ramaganthan, B.; Gopiraman, M.; Olasunkanmi, L. O.; Kabanda, M. M.; Yesudass, S.; Bahadur, I.; Adekunle, A. S.; Obot, I. B.; Ebenso, E. E. Synthesized Photo-Cross-Linking Chalcones as Novel Corrosion Inhibitors for Mild Steel in Acidic Medium: Experimental, Quantum Chemical and Monte Carlo Simulation Studies. *RSC Adv.* **2015**, *5* (94), 76675–76688. https://doi.org/10.1039/C5RA12097G.

(4) Gaur, R.; Gupta, V. K.; Pal, A.; Darokar, M. P.; Bhakuni, R. S.; Kumar, B. In Vitro and in Vivo Synergistic Interaction of Substituted Chalcone Derivatives with Norfloxacin against Methicillin Resistant Staphylococcus Aureus. *RSC Adv.* **2015**, *5* (8), 5830–5845. https://doi.org/10.1039/C4RA10842F.

(5) Moura, N. M. M.; Núñez, C.; Faustino, M. A. F.; Cavaleiro, J. A. S.; Neves, M. G. P. M. S.; Capelo, J. L.; Lodeiro, C. Preparation and Ion Recognition Features of Porphyrin–chalcone Type Compounds as Efficient Red-Fluorescent Materials. *J. Mater. Chem. C* **2014**, *2* (24), 4772–4783. https://doi.org/10.1039/C3TC32496F.

(6) Muhammad, S.; Xu, H.-L.; Zhong, R.-L.; Su, Z.-M.; Al-Sehemi, A. G.; Irfan, A. Quantum Chemical Design of Nonlinear Optical Materials by Sp2-Hybridized Carbon Nanomaterials: Issues and Opportunities. *J. Mater. Chem. C* **2013**, *1* (35), 5439. https://doi.org/10.1039/c3tc31183j.

(7) Moloney, J. V.; Newell, A. C. Nonlinear Optics. *Phys. D Nonlinear Phenom.* **1990**, *44* (1–2), 1–37. https://doi.org/10.1016/0167-2789(90)90045-Q.

(8) G. Papadopoulos, Manthos, Sadlej, Andrzej J., Leszczynski, J. *Non-Linear Optical Properties of Matter*; Papadopoulos, M. G., Sadlej, A. J., Leszczynski, J., Eds.; Springer Netherlands: Dordrecht, 2006. https://doi.org/10.1007/1-4020-4850-5.

(9) Schneider, T. *Nonlinear Optics in Telecommunications*; Advanced Texts in Physics; Springer Berlin Heidelberg: Berlin, Heidelberg, 2004. https://doi.org/10.1007/978-3-662-08996-5.

(10) Muhammad, S.; Irfan, A.; Shkir, M.; Chaudhry, A. R.; Kalam, A.; AlFaify, S.; Al-Sehemi, A. G.; Al-Salami, A. E.; Yahia, I. S.; Xu, H.-L.; et al. How Does Hybrid Bridging Core Modification Enhance the Nonlinear Optical Properties in Donor-π-Acceptor Configuration? A Case Study of Dinitrophenol Derivatives. *J. Comput. Chem.* **2015**, *36* (2), 118–128. https://doi.org/10.1002/jcc.23777.

(11) Muhammad, S.; Al-Sehemi, A. G.; Su, Z.; Xu, H.; Irfan, A.; Chaudhry, A. R. First Principles Study for the Key Electronic, Optical and Nonlinear Optical Properties of Novel Donor-Acceptor Chalcones. *J. Mol. Graph. Model.* **2017**, *72*, 58–69. https://doi.org/10.1016/j.jmgm.2016.12.009.

(12) Muhammad, S.; Al-Sehemi, A. G.; Irfan, A.; Chaudhry, A. R. Tuning the Push–pull Configuration for Efficient Second-Order Nonlinear Optical Properties in Some Chalcone Derivatives. *J. Mol. Graph. Model.* **2016**, *68*, 95–105. https://doi.org/10.1016/j.jmgm.2016.06.012.

(13) Mazzone, G.; Malaj, N.; Galano, A.; Russo, N.; Toscano, M. Antioxidant Properties of Several Coumarin–chalcone Hybrids from Theoretical Insights. *RSC Adv.* **2015**, *5* (1), 565–575. https://doi.org/10.1039/C4RA11733F.

(14) Wei, H.; Ruan, J.; Zhang, X. Coumarin–chalcone Hybrids: Promising Agents with Diverse Pharmacological Properties. *RSC Adv.* **2016**, *6* (13), 10846–10860. https://doi.org/10.1039/C5RA26294A.

(15) Custodio, J. M. F.; Santos, F. G.; Vaz, W. F.; Cunha, C. E. P.; Silveira, R. G.; Anjos, M. M.; Campos, C. E. M.; Oliveira, G. R.; Martins, F. T.; da Silva, C. C.; et al. Molecular Structure of Hybrid Imino-Chalcone in the Solid State: X-Ray Diffraction, Spectroscopy Study and Third-Order Nonlinear Optical Properties. *J. Mol. Struct.* **2018**, *1157*, 210–221. https://doi.org/10.1016/j.molstruc.2017.12.023.

(16) Aneja, B.; Arif, R.; Perwez, A.; Napoleon, J. V.; Hasan, P.; Rizvi, M. M. A.; Azam, A.; Rahisuddin; Abid, M. N-Substituted 1,2,3-Triazolyl-Appended Indole-Chalcone Hybrids as Potential DNA Intercalators Endowed with Antioxidant and Anticancer Properties. *ChemistrySelect* **2018**, *3* (9), 2638–2645. https://doi.org/10.1002/slct.201702913.

(17) Gupta, S.; Maurya, P.; Upadhyay, A.; Kushwaha, P.; Krishna, S.; Siddiqi, M. I.; Sashidhara, K. V.; Banerjee, D. Synthesis and Bio-Evaluation of Indole-Chalcone Based Benzopyrans as Promising Antiligase and Antiproliferative Agents. *Eur. J. Med. Chem.* **2018**, *143*, 1981–1996.

https://doi.org/10.1016/j.ejmech.2017.11.015.

(18) Domínguez, J. N.; León, C.; Rodrigues, J.; Gamboa, N.; Domínguez, D. Synthesis and Antimalarial Activity of Sulfonamide Chalcone Derivatives. *Farm.* **2005**, *60*, 307–311. https://doi.org/10.1016/j.farmac.2005.01.005.

(19) Eldehna, W. M.; Abo-Ashour, M. F.; Nocentini, A.; Gratteri, P.; Eissa, I. H.; Fares, M.; Ismael, O. E.; Ghabbour, H. A.; Elaasser, M. M.; Abdel-Aziz, H. A.; et al. Novel 4/3-((4-Oxo-5-(2-Oxoindolin-3-Ylidene)Thiazolidin-2-Ylidene)Amino) Benzenesulfonamides: Synthesis, Carbonic Anhydrase Inhibitory Activity, Anticancer Activity and Molecular Modelling Studies. *Eur. J. Med. Chem.* **2017**, *139*, 250–262. https://doi.org/10.1016/j.ejmech.2017.07.073.

(20) Ejaz, S. A.; Saeed, A.; Siddique, M. N.; Nisa, Z. un; Khan, S.; Lecka, J.; Sévigny, J.; Iqbal, J. Synthesis, Characterization and Biological Evaluation of Novel Chalcone Sulfonamide Hybrids as Potent Intestinal Alkaline Phosphatase Inhibitors. *Bioorg. Chem.* **2017**, *70*, 229–236. https://doi.org/10.1016/j.bioorg.2017.01.003.

(21) Kobkeatthawin, T.; Chantrapromma, S.; Chidan Kumar, C. S.; Fun, H.-K. Synthesis, Characterization, and Crystal Structure of Sulfonamide Chalcone: (E)-4-Methoxy-N-(4-(3-(3,4,5-Trimethoxyphenyl)Acryloyl)Phenyl)-Benzenesulfonamide. *Crystallogr. Reports* **2015**, *60* (7), 1058–1064. https://doi.org/10.1134/S1063774515070135.

(22) Custodio, J.; Michelini, L.; Castro, M.; Fonseca Vaz, W.; Neves, B. J.; Cravo, P.; Barreto, F.; de Moraes, M. O.; Perez, C.; Napolitano, H. Structural Insights on a Novel Anticancer Sulfonamide Chalcone. *New J. Chem.* **2018**, 1–9. https://doi.org/10.1039/C7NJ03523C.

(23) De Castro, M. R. C.; Aragão, Â. Q.; Da Silva, C. C.; Perez, C. N.; Queiroz, D. P. K.; Júnior, L. H. K. Q.; Barreto, S.; De Moraes, M. O.; Martins, F. T. Conformational Variability in Sulfonamide Chalcone Hybrids: Crystal Structure and Cytotoxicity. *J. Braz. Chem. Soc.* **2016**, *27* (5), 884–898. https://doi.org/10.5935/0103-5053.20150341.

(24) de Castro, M. R. C.; Naves, R. F.; Bernardes, A.; da Silva, C. C.; Perez, C. N.; Moura, A. F.; de Moraes, M. O.; Martins, F. T. Tandem Chalcone-Sulfonamide Hybridization, Cyclization and Further Claisen–Schmidt Condensation: Tuning Molecular Diversity through Reaction Time and Order and Catalyst. *Arab. J. Chem.* **2017**. https://doi.org/10.1016/j.arabjc.2017.11.005.

(25) Custodio, J. M. F.; Vaz, W. F.; de Castro, M. R. C.; Bernardes, A.; Naves, R. F.; Moura, A. F.; de Moraes, M. O.; da Silva, C. C.; Martins, F. T.; Perez, C. N.; et al. Solvent-Driven Structural Adaptation in a Novel Anticancer Sulfonamide Chalcone. *J. Mol. Struct.* **2019**, *1175*, 389–397.

https://doi.org/10.1016/j.molstruc.2018.07.059.

(26) Gu, B.; Ji, W.; Patil, P. S.; Dharmaprakash, S. M. Ultrafast Optical Nonlinearities and Figures of Merit in Acceptor-Substituted 3,4,5-Trimethoxy Chalcone Derivatives: Structure-Property Relationships. *J. Appl. Phys.* **2008**, *103* (10), 103511. https://doi.org/10.1063/1.2924419.

(27) D'silva, E. D.; Podagatlapalli, G. K.; Rao, S. V.; Rao, D. N.; Dharmaprakash, S. M. New, High Efficiency Nonlinear Optical Chalcone Co-Crystal and Structure–Property Relationship. *Cryst. Growth Des.* **2011**, *11* (12), 5362–5369. https://doi.org/10.1021/cg2009539.

(28) Arshad, M. N.; Al-Dies, A.-A. M.; Asiri, A. M.; Khalid, M.; Birinji, A. S.; Al-Amry, K. A.; Braga, A. A. C. Synthesis, Crystal Structures, Spectroscopic and Nonlinear Optical Properties of Chalcone Derivatives: A Combined Experimental and Theoretical Study. *J. Mol. Struct.* **2017**, *1141*, 142–156. https://doi.org/10.1016/j.molstruc.2017.03.090.

(29) Kajamuhideen, M. S.; Sethuraman, K.; Ramamurthi, K.; Ramasamy, P. Growth and Physical Characterization of Organic Nonlinear Optical Single Crystal: N,N′-Diphenylguanidinium Formate. *Opt. Laser Technol.* **2017**, *91*, 159–165. https://doi.org/10.1016/j.optlastec.2016.12.027.

(30) Wyss, S.; Werner, I. A.; Schweizer, W. B.; Ametamey, S. M.; Milicevic Sephton, S. Preparation and Structural Analysis of (±)-Threo-Ritalinic Acid. *Acta Crystallogr. Sect. C Cryst. Struct. Commun.* **2013**, *69* (11), 1225–1228. https://doi.org/10.1107/S010827011302595X.

(31) Li, C.; Ji, Y.; Cao, Q.; Li, J.; Li, B. Concise and Facile Synthesis of (*R,R*)-Dexmethylphenidate Hydrochloride and Its Three Stereoisomers. *Synth. Commun.* **2017**, *47* (14), 1301–1306. https://doi.org/10.1080/00397911.2017.1293109.

(32) Kim, J. H.; Ryu, W.; Shim, H.; Park, H. Development of New and Selective Trypanosoma Cruzi Trans-Sialidase Inhibitors from Sulfonamide Chalcones and Their Derivatives. *ChemBioChem* **2009**, *701*, 2475–2479. https://doi.org/10.1002/cbic.200900108.

(33) d'Oliveira, G.; Moura, A.; de Moraes, M.; Perez, C.; Lião, L. Synthesis, Characterization and Evaluation of in Vitro Antitumor Activities of Novel Chalcone-Quinolinone Hybrid Compounds. *J. Braz. Chem. Soc.* **2018**, *29* (11), 2308–2325. https://doi.org/10.21577/0103-5053.20180108.

(34) Sheldrick, G. M. A Short History of *SHELX*. *Acta Crystallogr. Sect. A Found. Crystallogr.* **2008**, *64* (1), 112–122. https://doi.org/10.1107/S0108767307043930.

(35) Sheldrick, G. M. Crystal Structure Refinement with SHELXL. *Acta Crystallogr. Sect. C Struct. Chem.* **2015**, *71* (1), 3–8. https://doi.org/10.1107/S2053229614024218.

(36) Spek, A. L. Single-Crystal Structure Validation with the Program PLATON. *J. Appl. Crystallogr.* **2003**, *36* (1), 7–13. https://doi.org/10.1107/S0021889802022112.

(37) Nardelli, M. PARST95 – an Update to PARST: A System of Fortran Routines for Calculating Molecular Structure Parameters from the Results of Crystal Structure Analyses. *J. Appl. Crystallogr.* **1995**, *28* (5), 659–659. https://doi.org/10.1107/S0021889895007138.

(38) Farrugia, L. J. WinGX and ORTEP for Windows: An Update. *J. Appl. Crystallogr.* **2012**, *45* (4), 849–854. https://doi.org/10.1107/S0021889812029111.

(39) Macrae, C. F.; Edgington, P. R.; McCabe, P.; Pidcock, E.; Shields, G. P.; Taylor, R.; Towler, M.; van de Streek, J. *Mercury* : Visualization and Analysis of Crystal Structures. *J. Appl. Crystallogr.* **2006**, *39* (3), 453–457. https://doi.org/10.1107/S002188980600731X.

(40) Sheik-Bahae, M.; Said, A. A.; Wei, T.-H.; Hagan, D. J.; Stryland, E. W. Van. Sensitive Measurement of Optical Nonlinearities Using a Single Beam. *IEEE J. Quantum Electron.* **1990**, *26* (4), 760–769. https://doi.org/10.1109/3.53394.

(41) Göppert-Mayer, M. Elementary Processes with Two Quantum Transitions. *Ann. der Phisik* **2009**, *18* (7–8), 466–479. https://doi.org/10.1002/andp.200910358.

(42) Clays, K.; Persoons, A. Hyper-Rayleigh Scattering in Solution. *Rev. Sci. Instrum.* **1992**, *63* (6), 3285–3289. https://doi.org/10.1063/1.1142538.

(43) Franzen, P. L.; Misoguti, L.; Zilio, S. C. Hyper-Rayleigh Scattering with Picosecond Pulse Trains. *Appl. Opt.* **2008**, *47* (10), 1443. https://doi.org/10.1364/AO.47.001443.

(44) Costero, A. M.; Betancourt-Mendiola, M. L.; Gaviña, P.; Ochando, L. E.; Gil, S.; Chulvi, K.; Peña-Cabrera, E. Structure and Conformational Studies of Aza-Crown 8-Amino-BODIPY Derivatives: Influence of Steric Hindrance on Their Photophysical Properties. *European J. Org. Chem.* **2017**, *2017* (42), 6283–6290. https://doi.org/10.1002/ejoc.201701016.

(45) da Costa, R.; Farias, F.; Maqueira, L.; Castanho Neto, C.; Carneiro, L.; Almeida, J.; Buarque, C.; Aucélio, R.; Limberger, J. Synthesis, Photophysical and Electrochemical Properties of Novel D-π-D and D-π-A Triphenylamino-Chalcones and β-Arylchalcones. *J. Braz. Chem. Soc.* **2019**, *30* (1), 81–89. https://doi.org/10.21577/0103-5053.20180156.

(46) Fonseca, R. D.; Vivas, M. G.; Silva, D. L.; Eucat, G.; Bretonnière, Y.; Andraud, C.; De Boni, L.; Mendonça, C. R. First-Order Hyperpolarizability of Triphenylamine Derivatives Containing Cyanopyridine: Molecular Branching Effect. *J. Phys. Chem. C* **2018**, *122* (3), 1770–1778. https://doi.org/10.1021/acs.jpcc.7b05829.

(47) Onsager, L. Electric Moments of Molecules in Liquids. *J. Am. Chem. Soc.* **1936**, *58* (8), 1486–1493. https://doi.org/10.1021/ja01299a050.

(48) Kamada, K.; Ohta, K.; Iwase, Y.; Kondo, K. Two-Photon Absorption Properties of Symmetric Substituted Diacetylene: Drastic Enhancement of the Cross Section near the One-Photon Absorption Peak. *Chem. Phys. Lett.* **2003**, *372* (3–4), 386–393. https://doi.org/10.1016/S0009-2614(03)00413-5.

(49) Neves, U. M.; De Boni, L.; Ye, Z.; Bu, X. R.; Mendonça, C. R. Two-Photon Absorption Spectra of Salen Dye Complexes with Azo Dyes. *Chem. Phys. Lett.* **2007**, *441* (4–6), 221–225. https://doi.org/10.1016/j.cplett.2007.05.021.

(50) Abegão, L. M. G.; Fonseca, R. D.; Santos, F. A.; Souza, G. B.; Barreiros, A. L. B. S.; Barreiros, M. L.; Alencar, M. A. R. C.; Mendonça, C. R.; Silva, D. L.; De Boni, L.; et al. Second- and Third-Order Nonlinear Optical Properties of Unsubstituted and Mono-Substituted Chalcones. *Chem. Phys. Lett.* **2016**, *648*, 91–96. https://doi.org/10.1016/j.cplett.2016.02.009.

(51) Lemes, S. R.; Júnior, L. A.; da Silva Manoel, D.; de Sousa, M. A. M.; Fonseca, R. D.; Lima, R. S.; Noda-Perez, C.; de Melo Reis, P. R.; Cardoso, C. G.; de Paula Silveira-Lacerda, E.; et al. Optical Properties and Antiangiogenic Activity of a Chalcone Derivate. *Spectrochim. Acta Part A Mol. Biomol. Spectrosc.* **2018**, *204*, 685–695. https://doi.org/10.1016/j.saa.2018.06.099.

(52) Custodio, J. M. F.; D'Oliveira, G. D. C.; Gotardo, F.; Cocca, L. H. Z.; De Boni, L.; Perez, C. N.; Maia, L. J. Q.; Valverde, C.; Osório, F. A. P.; Napolitano, H. B. Chalcone as Potential Nonlinear Optical Material: A Combined Theoretical, Structural, and Spectroscopic Study. *J. Phys. Chem. C* **2019**, *123* (10), 5931–5941. https://doi.org/10.1021/acs.jpcc.9b01063.

(53) Santos, F. A.; Abegão, L. M. G.; Fonseca, R. D.; Alcântara, A. M.; Mendonça, C. R.; Valle, M. S.; Alencar, M. A. R. C.; Kamada, K.; De Boni, L.; Rodrigues, J. J. Bromo-and Chloro-Derivatives of Dibenzylideneacetone: Experimental and Theoretical Study of the First Molecular Hyperpolarizability and Two-Photon Absorption. *J. Photochem. Photobiol. A Chem.* **2019**, *369*, 70–76. https://doi.org/10.1016/j.jphotochem.2018.10.012.

(54) Oudar, J. L. Optical Nonlinearities of Conjugated Molecules. Stilbene Derivatives and Highly Polar Aromatic Compounds. *J. Chem. Phys.* **1977**, *67* (2), 446–457. https://doi.org/10.1063/1.434888.

(55) Campo, J.; Wenseleers, W.; Goovaerts, E.; Szablewski, M.; Cross, G. H. Accurate Determination and Modeling of the Dispersion of the First Hyperpolarizability of an Efficient Zwitterionic

Nonlinear Optical Chromophore by Tunable Wavelength Hyper-Rayleigh Scattering. *J. Phys. Chem. C* **2008**, *112* (1), 287–296. https://doi.org/10.1021/jp0758824.

(56) Orr, B. J.; Ward, J. F. Perturbation Theory of the Non-Linear Optical Polarization of an Isolated System. *Mol. Phys.* **1971**, *20* (3), 513–526. https://doi.org/10.1080/00268977100100481.